Hindawi Publishing Corporation
Journal of Nanomaterials
Volume 2015, Article ID 704817, 7 pages
http://dx.doi.org/10.1155/2015/704817

Research Article

Targeted *In Vivo* Imaging of Mouse Hindlimb Ischemia Using Fluorescent Gelatin Nanoparticles

Ju Zhang,[1] Gang Wang,[1] Duo Mao,[1] Aitian Han,[1] Nannan Xiao,[1] Xin Qi,[2] Dan Ding,[1] and Deling Kong[1]

[1]*State Key Laboratory of Medicinal Chemical Biology, Key Laboratory of Bioactive Materials, Ministry of Education, College of Life Sciences, and Collaborative Innovation Center of Chemical Science and Engineering (Tianjin), Nankai University, Tianjin 300071, China*
[2]*Tianjin Union Medicine Center (Nankai University Affiliated Hospital), Clinical and Translation Medicine Lab, Tianjin 300121, China*

Correspondence should be addressed to Xin Qi; qixinx2011@126.com and Dan Ding; dingd@nankai.edu.cn

Received 16 October 2014; Accepted 17 December 2014

Academic Editor: Shuming Zhang

Critical limb ischemia is one of the most advanced forms of peripheral artery disease, which seriously threat the human health and even cause amputation. In this study, we developed a fluorescent gelatin nanoparticle (FGNP) by covalent conjugation of the nanoparticles with two fluorogens, Cy7 and rhodamine B. The FGNPs have a volume average hydrodynamic diameter of about 168 nm, which also show low cytotoxicity against NIH/3T3 normal cells. The *in vivo* ischemia bioimaging studies in live mice and in ischemic limb slices demonstrate that the FGNPs can be preferentially accumulated to the ischemic site, which can thus serve as a safe and effective probe for targeted visualization of ischemia in the limb.

1. Introduction

The research on biocompatible nanomaterials for diagnosis and treatment of diseases has attracted increasing interest, as these nanomaterials exhibit the merits of improved water solubility of hydrophobic therapeutic/imaging agents, targeted delivery of the agents in a cell- or tissue-specific manner, and codelivery of both treatment and imaging agents for simultaneous theranostics [1–3]. Ischemic disease refers to the restriction in blood supply to tissues/organs, which would result in the damage to or dysfunction of tissues and may lead to tissue death. Ischemic disease would occur in a variety of tissues including heart (myocardial infarction), bowel (ischemic colitis and mesenteric ischemia), brain (stroke), skin (cyanosis), and limb (critical limb ischemia). Among them, critical limb ischemia is one of the most advanced forms of peripheral artery disease, which seriously threat the human health and even cause amputation [4, 5]. In the past decades, however, considerable efforts have been made on the nanotechnology systems aimed at therapeutics and diagnostics of cancer. There have been very few works focused on the treatment and imaging of ischemic limb disease using biocompatible nanomaterials [6]. As a consequence, the unique advantages of nanotechnology motivate us to explore biocompatible nanomaterials to address some issues in the field of ischemic limb disease.

Biocompatible and biodegradable polymeric nanoparticles have been extensively investigated in recent years for both therapeutic and diagnostic purposes of cancers, which hold great promise as reliable, effective, and safe systems for *in vivo* applications and further clinical translation [7]. Many types of polymeric nanomaterials such as self-assembling synthetic polymers, polysaccharide, and protein nanoparticles have shown their uniqueness in various biomedical utilities [8, 9]. Among these colloidal systems, protein-based nanomaterials have received great attention as they have the advantages of less immunogenicity, nontoxicity, facile preparation, and long-term storage stability. Besides, protein-based nanomaterials are also allowed for flexible surface functionalization by virtue of the large number of pendant functional groups in the protein structure [10, 11]. As a naturally occurring protein, gelatin that is obtained by hydrolytic degradation

of collagen has a long history of safe applications in the areas of medicine, cosmetics, and food [12–14]. Due to the aforementioned reasons, gelatin was selected in the present study as the starting material to fabricate biocompatible fluorescent nanoparticles.

In this contribution, we report the preparation of fluorescent gelatin nanoparticles (FGNPs), which can target visualization of the ischemia in the mouse hind limb. The gelatin nanoparticles were synthesized via a two-desolvation method [13, 14], which were subsequently covalently conjugated with two fluorogens, cy7 and rhodamine B, in order to trace the gelatin nanoparticles in both noninvasive manner and single-cell resolution. The imaging studies in a mouse ischemic hind limb model reveal that FGNPs can be preferentially accumulated into the ischemic muscles from blood circulation. This study thus offers fundamental guidelines to use biocompatible nanomaterials for the treatment and diagnosis of ischemic diseases, which will inspire more exciting research in this emerging field.

2. Materials and Methods

2.1. Materials. Gelatin type A from porcine skin (175 Bloom Sigma-Aldrich, Steinheim, Germany) and rhodamine B isothiocyanate were purchased from Sigma Aldrich. Cy7 NHS ester was obtained from Lumiprobe Co., Ltd. All the other starting materials were obtained from Alfa. Commercially available reagents were used without further purification, unless noted otherwise.

2.2. Characterization. UV-vis spectra were recorded on a Shimadzu UV-1700 spectrometer. Emission spectra were recorded on a Perkin-Elmer LS 55 spectrofluorometer. The nanoparticle size was measured with Zetasizer Nano ZS (Nano-ZS, MALVERN). The morphology of the nanoparticles was studied by scanning electron microscopy (SEM, JSM-6700F, JEOL, Japan) at an accelerating voltage of 10 kV. The sample was fixed on a stub with a double-sided sticky tape and then coated with a platinum layer using an autofine coater (JEOL, Tokyo, Japan) for 60 s in vacuum at a current intensity of 10 mA. The morphology of NPs was also investigated by transmission electron microscopy (TEM, JEM-2010F, JEOL, Japan).

2.3. Preparation of FGNPs. 1 g of gelatin powder was dissolved in 20 mL of deionized water under magnetic stirring at 40°C. Subsequently, a large amount of acetone was added to achieve the desolvation and rapid sedimentation of the gelatin. After discarding the supernatant, the gelatin colloid was redissolved in 20 mL of deionized water. The pH value of the solution was adjusted to 2.7 using a 1 M HCl solution. The gelatin nanoparticles were formed by controlled precipitation of the aqueous gelatin solution with acetone under continuous stirring. After that, 7.5 μL of 50% glutaraldehyde was added to cross-link the gelatin nanoparticles, which was allowed to be stirred overnight. The gelatin nanoparticle suspension was purified by ultrafiltration (molecule weight cutoff 12 kDa) to remove the acetone and extra cross-linker. The stock solution of gelatin nanoparticles was prepared at the concentration of 5 mg/mL. To prepare FGNPs, Cy7 NHS ester was dissolved in DMSO at 1 mg/mL. The suspension of gelatin nanoparticles was adjusted to pH around 8.0 by 0.2 N of sodium hydroxide solution. Subsequently, 100 μL of the dye solution was added to 2 mL of the gelatin nanoparticle stock solution, which was agitated gently for 12 h. The Cy7-labeled gelatin nanoparticles were purified by ultrafiltration (molecule weight cutoff 12 kDa) to remove unconjugated Cy7. The rhodamine B isothiocyanate was also labeled to the gelatin nanoparticles under the same procedure.

2.4. Cell Viability Assay. Cytotoxicity of the FGNPs was evaluated with mouse NIH/3T3 cells using a cell counting kit-8 (CCK-8) viability assay. In this experiment, the cells were divided into two groups, the control group and the sample group. In detail, the cells were seeded with a density of 5×10^3 cells/well in 96-well microtiter plates and preincubated for 24 h under 5% CO_2 in the cell incubator at 37°C using DMEM cell culture media (Hyclone). The cells in sample group were then treated with a series of concentrations of FGNPs. After 24 h incubation, 10 μL of CCK-8 (Dojindo, Japan) solution that was predissolved in cell culture medium was added to each well. After incubation for 40 min, the absorbance of each well was measured by a microplate reader (Thermo Scientific Varioskan Flash) at the wavelength of 450 nm. The proliferation rates of NIH/3T3 cells after incubation with FGNPs were presented as the ratio of absorbance of cells in sample group to that of cells in control group. There were six parallel samples in each group.

2.5. Bioimaging in a Mouse Ischemic Hind Limb Model. All animal studies were conducted under a protocol approved by Nankai University. ICR mice (20–30 g, 8–10 weeks old) were purchased from Vital River Laboratory Animal Technology Co., Ltd. (Beijing, China). The mice were anesthetized by intraperitoneal injection of 4% chloral hydrate solution at a dosage of 8 μL per gram body weight. Unilateral hind limb ischemia in the left leg was induced in male ICR mice by ligation and excision of the right femoral artery distal to the inguinal ligament. The ischemic limb-bearing mice were then injected with 200 μL of FGNPs via the tail vein. The mice were then anesthetized and placed on an animal plate heated to 37°C. The time-dependent biodistribution of the FGNPs in ischemic limb-bearing mice was imaged using a Maestro EX *in vivo* fluorescence imaging system (CRi, Inc.). The light with a central wavelength at 735 nm was selected as the excitation source. *In vivo* spectral imaging from 780 nm to 950 nm (10 nm step) was carried out with an exposure time of 150 ms for each image frame. The autofluorescence was removed using spectral unmixing software. Scans were carried out at 4 h and 24 h after injection, respectively. In addition, at 4 h and 24 h after injection, respectively, the ischemic limb-bearing mice intravenously injected with FGNPs were sacrificed and the tissues including spleen, liver, lung, kidney, and ischemic and nonischemic limbs were isolated and imaged using the Maestro system. The average fluorescence intensity of each harvested tissue ($n = 3$ mice per group) was calculated for a semiquantitative biodistribution study using the Maestro software.

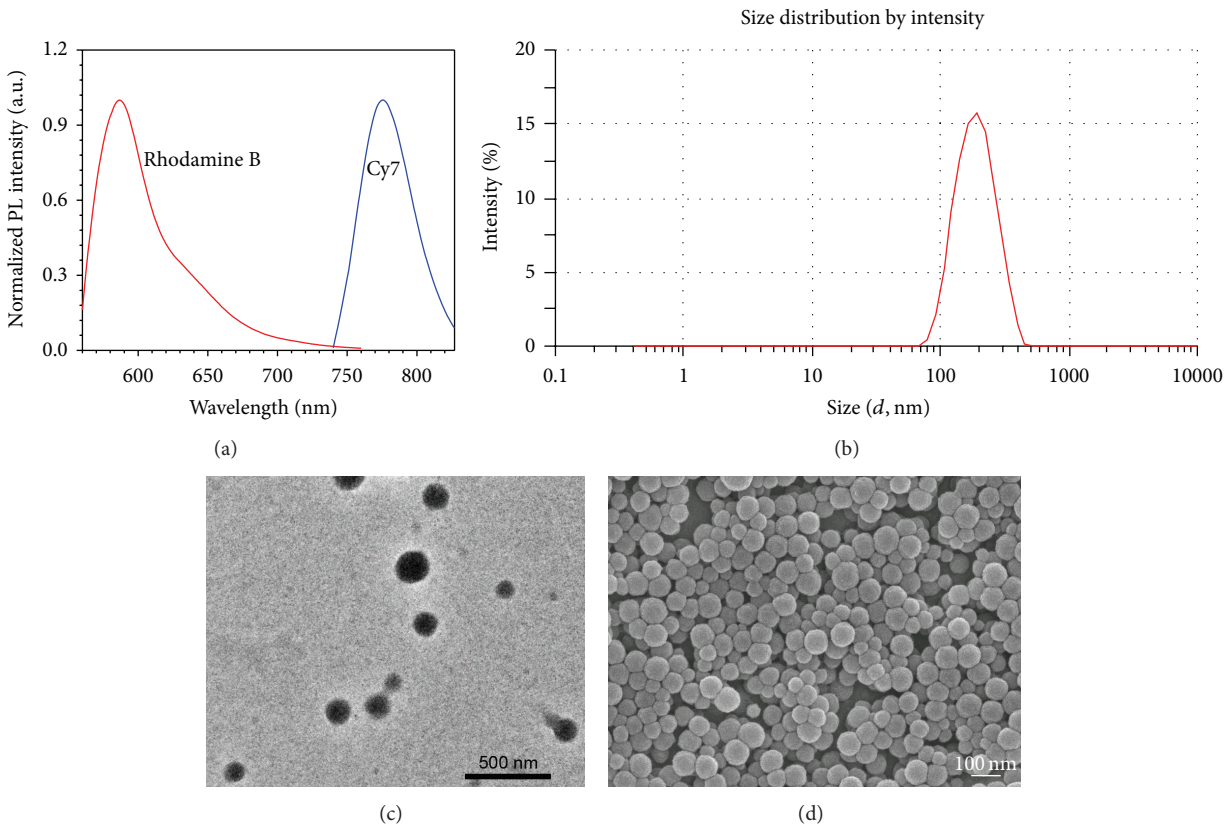

Figure 1: (a) Photoluminescence spectra of FGNPs in water upon excitation at 543 nm (for rhodamine B) and 735 nm (for Cy7), respectively. (b) Size distribution of FGNPs measured by DLS. (c) TEM and (d) SEM images of FGNPs.

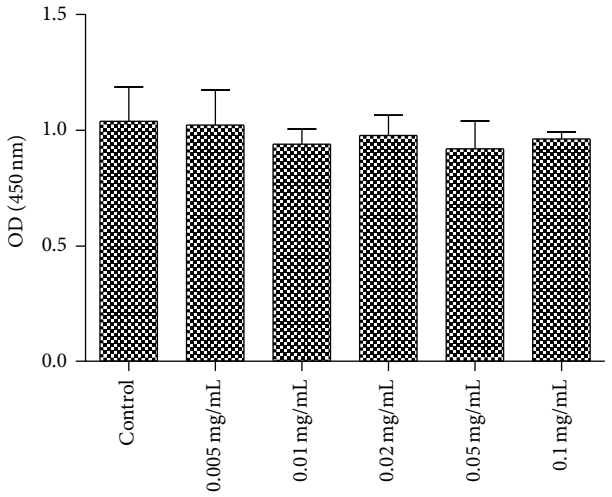

Figure 2: Proliferation rates of NIH/3T3 cells after incubation with FGNPs at various concentrations for 24 h by CCK-8 assay.

2.6. Immunostaining Study. To investigate the distribution of FGNPs in relation to blood vessels, the ischemic limb slices were obtained from the ischemic limb-bearing mice treated with FGNPs for 24 h. The ischemic limbs were fixed in 4% paraformaldehyde for 2 h, incubated in 20% sucrose/PBS overnight, and embedded in Optimal Cutting Temperature (OCT) compound (Tissue-Tek). Sections (6 μm) were immunostained with monoclonal

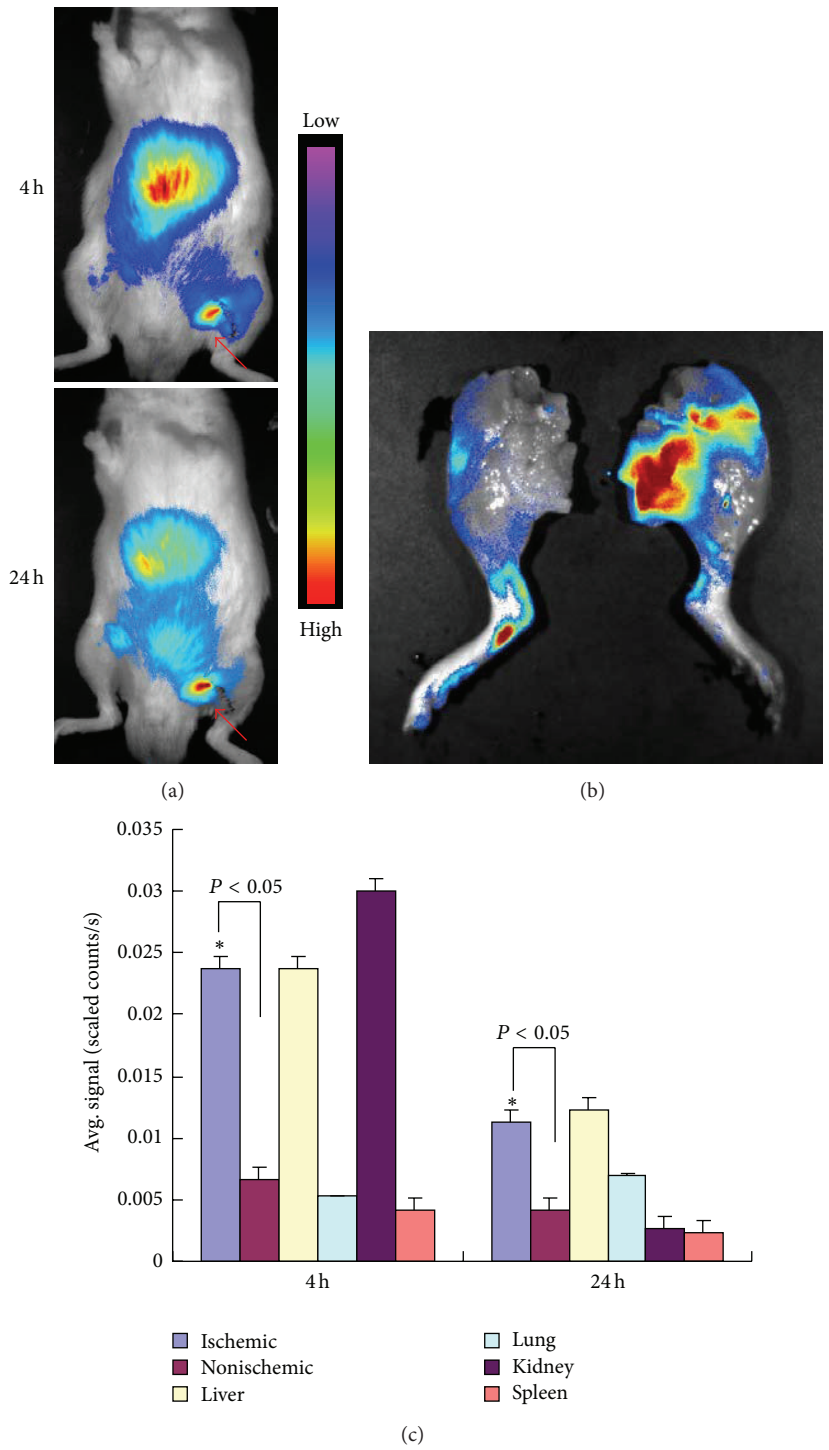

Figure 3: (a) *In vivo* noninvasive fluorescence imaging of ischemic limb-bearing mice after intravenous injection of FGNPs for 4 h and 24 h, respectively. The red arrows indicate the ischemic site. (b) *Ex vivo* fluorescence imaging of ischemic and nonischemic limbs from mice treated with FGNPs for 24 h. (c) Semiquantitative biodistribution analysis of FGNPs in the indicated tissues at 4 h and 24 h after injection, respectively. Data are presented as mean ± standard deviation ($n = 3$). $*$ represents statistical significance ($P < 0.05$).

antibody against platelet/endothelial cell adhesion molecule 1 (PECAM-1; PharMingen). Alexa Fluor 488-conjugated anti-rat antibody was used as secondary antibody (Molecular Probes). The FGNPs were excited at 543 nm and the blood vessels were imaged upon excitation at 488 nm.

2.7. Histology Observation. The tissues including liver, spleen, and kidney from the ischemic limb-bearing mice that received FGNPs were selected for histology observation on the 7th day after injection ($n = 3$ mice per group). The organs were dissected and fixed in 10% neutral buffered

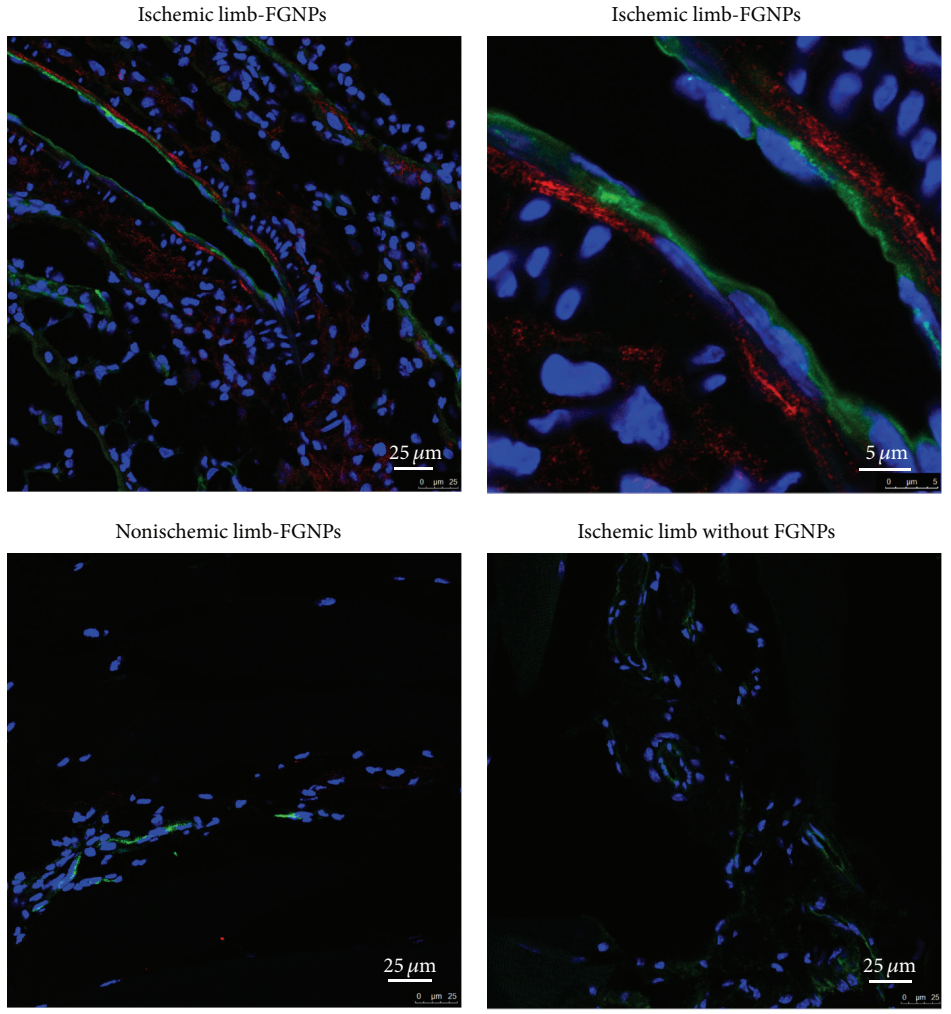

Figure 4: Confocal fluorescence images of ischemic and nonischemic limb slices from mice after intravenous injection with FGNPs for 24 h. The blood vessels were immunostained against platelet/endothelial cell adhesion molecule 1 (PECAM-1). The cell nuclei were stained with 4′,6-diamidino-2-phenylindole (DAPI).

formalin. Thereafter, the tissues were processed routinely into paraffin, sectioned at a thickness of 4 μm, and stained with hematoxylin and eosin (H&E). The slices obtained were examined by optical microscopy.

2.8. Statistical Analysis. Quantitative data were expressed as mean ± standard deviation. Statistical comparisons were made by ANOVA analysis and Student's t-test. P value < 0.05 was considered statistically significant.

3. Results and Discussion

3.1. Preparation and Characterization of FGNPs. Gelatin nanoparticles were prepared by the two-desolvation method through addition of acetone into gelatin aqueous solution, followed by nanoparticle cross-linking with glutaraldehyde. To track the gelatin nanoparticles *in vivo*, a near-infrared fluorescent dye, Cy7, was labeled to gelatin nanoparticles, allowing for noninvasive live animal imaging. Moreover, to visualize nanoparticles in tissue slices with single-cell resolution, rhodamine B was also conjugated to the nanoparticles, affording Cy7 and rhodamine B dual-labeled gelatin nanoparticles (FGNPs). The emission spectra of FGNPs in water upon excitation at 543 nm and 735 nm, respectively, are shown in Figure 1(a). The FGNPs have emission peaks centered at 587 nm and 776 nm, respectively, at each excitation wavelength, which demonstrates that the FGNPs are labeled with both fluorogens. The dynamic light scattering (DLS) result suggests that the FGNPs have a volume average hydrodynamic diameter of around 168 nm (Figure 1(b)). The zeta potential of the FGNPs is measured to be −1.6 mV. Transmission electron microscopy (TEM) and scanning electron microscopy (SEM) images of FGNPs are shown in Figures 1(c) and 1(d), which indicate that the FGNPs are spherical in shape with an average size of about 134 nm. This is smaller as compared to that determined by DLS owing to the shrinkage of nanoparticles in the dry state [15]. Furthermore, the cell proliferation rates of NIH/3T3 normal cells after incubation

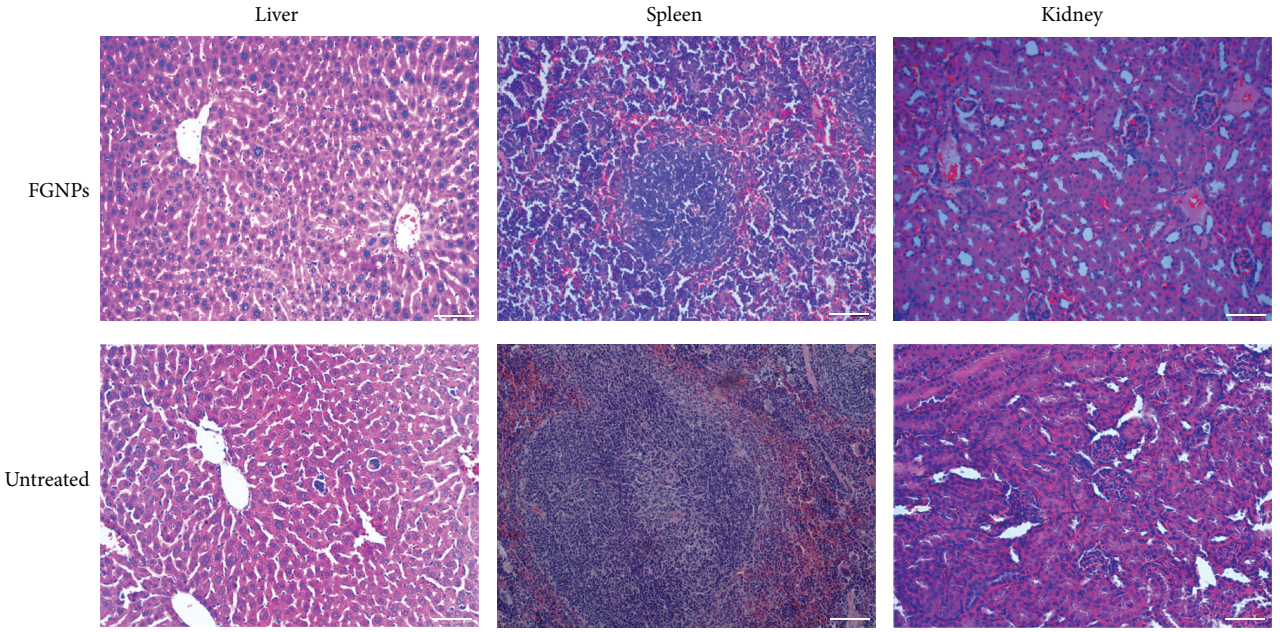

Figure 5: Typical images taken from H&E-stained liver, spleen, and kidney slices from mice treated with and without FGNPs. The scale bar is 100 μm.

with FGNPs at different concentrations for 24 h were quantitatively determined by the CCK-8 assay, as shown in Figure 2. The result indicates that the FGNPs are nontoxic against NIH/3T3 cells, suggesting that the FGNPs are biocompatible and promising for further *in vivo* applications.

3.2. Targeted Visualizing of Ischemia in the Mouse Limb. The application of FGNPs in imaging ischemic limb in live mice was also studied by the noninvasive live animal fluorescence imaging technique. In this experiment, a hind limb ischemia mouse model was established and employed. After intravenous injection with the FGNPs, the ischemic limb-bearing mice were imaged with a Maestro EX *in vivo* fluorescence imaging system. The light with a central wavelength at 735 nm was selected as the excitation source to excite Cy7 in the FGNPs. Through spectral unmixing utilizing the Maestro software, the mouse autofluorescence was removed. Figure 3(a) shows the *in vivo* distribution of FGNPs in the ischemic limb-bearing mice 4 h and 24 h after injection, respectively. As shown in Figure 3(a), the red arrows indicate the ischemic site and intense fluorescence signals are observed in the ischemic site of the mouse hind limb at both 4 h and 24 h after administration. The sharp fluorescence intensity contrast between ischemic and nonischemic limbs reveals that the FGNPs can serve as an effective probe for ischemic site visualization in a highly sensitive manner. The ability of the FGNPs to clearly illustrate the ischemic site should be ascribed from the enhanced permeability and retention (EPR) effect, known as "passive" targeting [16], thanks to the nanoscale size of the FGNPs. At 24 h after injection, the mice were sacrificed and the ischemic as well as nonischemic limbs were excised for *ex vivo* fluorescence imaging. As illustrated in Figure 3(b), the image demonstrates the prominent passive targeting capability of the FGNPs to the ischemic site.

Moreover, the main organs of the FGNP-administrated mice including liver, lung, kidney, and spleen were also excised and the average fluorescence signal of each harvested tissue at 4 h and 24 h after injection, respectively, was measured for a semiquantitative biodistribution analysis. As shown in Figure 3(c), besides the preferential accumulation in the ischemic limb, the FGNPs are mainly distributed in the liver and kidney tissues at 4 h after injection. With the time elapses, the fluorescence signals in both liver and kidney significantly decrease, indicating that the FGNPs can be excreted from the body by the corresponding pathways [17]. Furthermore, the difference in fluorescence intensity between ischemic and nonischemic limbs is statistically significant at both time points.

The ischemic and nonischemic limbs from mice after intravenous injection of FGNPs for 24 h were excised and sliced for immunostaining against platelet/endothelial cell adhesion molecule 1 (PECAM-1) in order to visualize the blood vessels in the limbs. As exhibited in Figure 4, it is obvious that the red fluorescence of FGNPs (from rhodamine B upon excitation at 543 nm) is localized near the blood vessels (green fluorescence). On the other hand, almost no detectable fluorescence signal from FGNPs can be observed near or close to the vasculature. These results reveal that the FGNPs can be accumulated into the ischemic site via the blood vessels in the ischemic muscle, confirming the prominent passive targeting ability of the FGNPs. As control, there is nearly no detectable red fluorescence in the slice of ischemic limb from mice without FGNP administration.

In addition, the main organs including liver, spleen, and kidney from mice injected with FGNPs were performed on for histological analyses. Figure 5 shows the optical images from hematoxylin and eosin- (H&E-) stained slices in these tissues, which indicate that the FGNPs would not cause any significant lesion to the normal organs compared with those from untreated mice, as verified by 3 independent pathologists. This result reveals that the FGNPs hold great potential to be a safe and effective nanoprobe for visualization of ischemia in the limb.

4. Conclusions

We report the synthesis and characterization of a fluorescent gelatin nanoparticle, which possesses a mean size of around 168 nm measured by DLS, low cytotoxicity, and ability to visualize ischemic limb in both noninvasive manner and single-cell resolution. We have demonstrated that the FGNPs can serve as a safe and efficient probe for imaging ischemic limb. This study will open up a new avenue for development of biocompatible nanomaterials in the therapeutics and diagnostics of ischemic diseases.

Conflict of Interests

The authors declare that there is no conflict of interests regarding the publication of this paper.

Authors' Contribution

Ju Zhang and Gang Wang contributed equally to this work.

Acknowledgments

This work was supported by grants from the National Basic Research Program of China (2011CB964903), NSFC (81220108015 and 81301311), and the Program for Changjiang Scholars and Innovative Research Team in University (IRT13023).

References

[1] X. Gao, Y. Cui, R. M. Levenson, L. W. K. Chung, and S. Nie, "*In vivo* cancer targeting and imaging with semiconductor quantum dots," *Nature Biotechnology*, vol. 22, no. 8, pp. 969–976, 2004.

[2] D. Ding, Z. Zhu, R. Li et al., "Nanospheres-incorporated implantable hydrogel as a trans-tissue drug delivery system," *ACS Nano*, vol. 5, no. 4, pp. 2520–2534, 2011.

[3] L. Lian, F. Tang, J. Yang, C. Liu, and Y. Li, "Therapeutic angiogenesis of PLGA-heparin nanoparticle in mouse ischemic limb," *Journal of Nanomaterials*, vol. 2012, Article ID 193704, 6 pages, 2012.

[4] H. N. Yang, J. S. Park, D. G. Woo, S. Y. Jeon, and K.-H. Park, "Transfection of $VEGF_{165}$ genes into endothelial progenitor cells and *in vivo* imaging using quantum dots in an ischemia hind limb model," *Biomaterials*, vol. 33, no. 33, pp. 8670–8684, 2012.

[5] Y. Li, W. Liu, F. Liu et al., "Primed 3D injectable microniches enabling low-dosage cell therapy for critical limb ischemia," *Proceedings of the National Academy of Sciences*, vol. 111, no. 37, pp. 13511–13516, 2014.

[6] J. Kim, L. Cao, D. Shvartsman, E. A. Silva, and D. J. Mooney, "Targeted delivery of nanoparticles to ischemic muscle for imaging and therapeutic angiogenesis," *Nano Letters*, vol. 11, no. 2, pp. 694–700, 2011.

[7] Z. Ge and S. Liu, "Functional block copolymer assemblies responsive to tumor and intracellular microenvironments for site-specific drug delivery and enhanced imaging performance," *Chemical Society Reviews*, vol. 42, no. 17, pp. 7289–7325, 2013.

[8] J.-H. Kim, Y.-S. Kim, K. Park et al., "Self-assembled glycol chitosan nanoparticles for the sustained and prolonged delivery of antiangiogenic small peptide drugs in cancer therapy," *Biomaterials*, vol. 29, no. 12, pp. 1920–1930, 2008.

[9] D. Ding, Z. Zhu, Q. Liu et al., "Cisplatin-loaded gelatin-poly(acrylic acid) nanoparticles: synthesis, antitumor efficiency *in vivo* and penetration in tumors," *European Journal of Pharmaceutics and Biopharmaceutics*, vol. 79, no. 1, pp. 142–149, 2011.

[10] M. G. Anhorn, S. Wagner, J. Kreuter, K. Langer, and H. von Briesen, "Specific targeting of HER2 overexpressing breast cancer cells with doxorubicin-loaded trastuzumab-modified human serum albumin nanoparticles," *Bioconjugate Chemistry*, vol. 19, no. 12, pp. 2321–2331, 2008.

[11] H. Wang, J. Liu, A. Han et al., "Self-assembly-induced far-red/near-infrared fluorescence light-up for detecting and visualizing specific protein-peptide interactions," *ACS Nano*, vol. 8, no. 2, pp. 1475–1484, 2014.

[12] C. L. Tseng, W. Y. Su, K. C. Yen, K. C. Yang, and F. H. Lin, "The use of biotinylated-EGF-modified gelatin nanoparticle carrier to enhance cisplatin accumulation in cancerous lungs *via* inhalation," *Biomaterials*, vol. 30, no. 20, pp. 3476–3485, 2009.

[13] C. Wong, T. Stylianopoulos, J. Cui et al., "Multistage nanoparticle delivery system for deep penetration into tumor tissue," *Proceedings of the National Academy of Sciences of the United States of America*, vol. 108, no. 6, pp. 2426–2431, 2011.

[14] G. Kaul and M. Amiji, "Long-circulating poly(ethylene glycol)-modified gelatin nanoparticles for intracellular delivery," *Pharmaceutical Research*, vol. 19, no. 7, pp. 1061–1067, 2002.

[15] D. Ding, C. C. Goh, G. Feng et al., "Ultrabright organic dots with aggregation-induced emission characteristics for real-time two-photon intravital vasculature imaging," *Advanced Materials*, vol. 25, no. 42, pp. 6083–6088, 2013.

[16] M. Morille, T. Montier, P. Legras et al., "Long-circulating DNA lipid nanocapsules as new vector for passive tumor targeting," *Biomaterials*, vol. 31, no. 2, pp. 321–329, 2010.

[17] Z. Liu, C. Davis, W. Cai, L. He, X. Chen, and H. Dai, "Circulation and long-term fate of functionalized, biocompatible single-walled carbon nanotubes in mice probed by Raman spectroscopy," *Proceedings of the National Academy of Sciences of the United States of America*, vol. 105, no. 5, pp. 1410–1415, 2008.